IEEE Access
Multidisciplinary ⋮ Rapid Review ⋮ Open Access Journal

Received August 13, 2020, accepted August 18, 2020, date of publication August 20, 2020, date of current version September 1, 2020.

Digital Object Identifier 10.1109/ACCESS.2020.3018297

Laser-Drilled All-Dielectric Huygens' Transmit-Arrays as 120 GHz Band Beamformers

MOHAMED K. EMARA[1], (Graduate Student Member, IEEE), SONYA K. STUHEC-LEONARD[1], (Student Member, IEEE), TAKASHI TOMURA[2], (Member, IEEE), JIRO HIROKAWA[2], (Fellow, IEEE), AND SHULABH GUPTA[1], (Senior Member, IEEE)

[1]Department of Electronics, Carleton University, Ottawa, ON K1S 5B6, Canada
[2]Department of Electrical and Electronic Engineering, Tokyo Institute of Technology, Tokyo 152-8552, Japan

Corresponding author: Mohamed K. Emara (mohamed.emara@carleton.ca)

This work was supported in part by the Support Center for Advanced Telecommunications Technology Research Foundation (SCAT), in part by the Mizuho Foundation for the Promotion of Sciences, and in part by the Natural Sciences and Engineering Research Council of Canada.

ABSTRACT An all-dielectric Huygens' transmit-array is proposed and experimentally demonstrated in the 120-GHz-band. The proposed transmit-array is fabricated using a high-precision laser-drilling process providing high fabrication precision and accuracy. A non-uniform Huygens' surface is next placed on top of a planar high gain slot-array antenna for far-field beamforming. Full-wave simulations are first used to demonstrate the beamforming capability by generating difference-pattern beams as an example. A uniform transmit-array was then fabricated and characterized to investigate the effect of the transmit-array on the antenna performance, along with showing very low fabrication tolerances and minimal dimensional variation due to the laser drilling process. Next, a phase-gradient transmit-array for beam-tilting is experimentally demonstrated as a practical example of beamforming. The proposed all-dielectric structure is the first Huygens' structure to be demonstrated at these frequency bands, and represents an attractive alternative to conventional metallic Huygens' metasurfaces based on standard printed circuit board (PCB) solutions.

INDEX TERMS 6G networks, all-dielectric metasurface, beamforming, difference-pattern, Huygens' transmit-array, laser-drilling, millimeter-wave (mm-wave), refraction, slot array antenna.

I. INTRODUCTION

Electromagnetic metasurfaces are 2-D structures that consist of arrays of sub-wavelength resonators [1]. A wide range of electromagnetic (EM) wave manipulations can be achieved by careful design of the geometric shapes and material properties of these resonators. For example, metasurfaces have been used for applications such as controlled reflection [2]–[4], polarization control [5]–[7], refraction [8]–[10], absorption [11]–[13], and electromagnetic illusions and cloaking [14], [15], using variety of resonator configurations. An important class of metasurface is a *Huygens' Metasurface*, which exhibits orthogonal and co-located electric and magnetic dipoles [16]–[18]. By exciting both dipole moments, a Huygens' metasurface can be synthesized to achieve wide variety of EM wave transformation with zero back-scattering, thus providing phase control in transmission.

Metasurfaces, and in particular Huygens' metasurfaces, can be broadly classified into two categories based on their design: metallic metasurfaces and all-dielectric metasurfaces. Metallic metasurfaces are composed of unit cells that consist of metallic patterns, most commonly implemented on a dielectric substrate using standard printed circuit board (PCB) processes, at microwaves [19]–[27]. On the other hand, all-dielectric metasurfaces, as the name suggests, are composed of unit cells based solely on dielectric materials [17], [28]–[42]. All-dielectric metasurfaces are preferred over metallic metasurfaces because they typically exhibit lower Ohmic losses as frequencies become higher, as typically observed at optical frequencies [43]. Various design techniques exist to design such surfaces, where for instance, all-dielectric metasurface have been modeled using deep neural networks [44] and analytical modeling

The associate editor coordinating the review of this manuscript and approving it for publication was Kuang Zhang.

of spherical particles [45], while metallic metasurfaces are modeled using typical circuit analysis [46].

Metallic metasurfaces are more common at microwave frequencies due to the mature PCB-based fabrication, however as frequency increases towards mm-waves and beyond 100 GHz, realizing narrow line-widths and gaps using standard PCB fabrication becomes challenging, in addition to associated Ohmic losses. Consequently, some efforts have been made to realize photonics inspired all-dielectric metasurface structures at microwaves [2], [28], [29], [31] and mm-wave frequencies [47], as an alternative to metallic resonator-based metasurfaces. Such structures are based on mechanically drilling typical substrate materials, as opposed to standard PCB processes, to form dielectric resonators connected using bridges. However, such structures based on single layer dielectrics do not scale to mm-wave frequencies due to mechanical vibrations induced during the drilling process, leading to large fabrication errors [48]. Consequently, a double layer all-dielectric structure with double cross bridged unit cell has recently been proposed in [47] at 60 GHz IEEE 801.11ad to mitigate this problem.

On the application side, with the upcoming sixth generation (6G) communication networks [49] being expected to see a high demand for antenna beamforming techniques above 100 GHz, there is an interest in devising novel ways to enable general wave transformations. It can either be in the form of novel antenna structures or achieving beam shaping using external phase plates realized using metasurfaces, for instance, where Huygens' metasurface can be used for engineering the near-field distribution of directive, high gain antennas [50]. Of particular interest in this work is operating in the near-field zone of large-scale antenna arrays used in the Gigabit Access Transponder Equipment (GATE) for short-range communication [51]. These antennas are designed using a complex and expensive process of diffusion-bonding of metallic plates so normally they are designed with a near-uniform phase to achieve broadside radiation in the far-field. There are two options to achieve other patterns shapes and directions. The first choice involves redesigning the antenna which is a challenging process. A second alternative is to use a metasurface operating in the near-field of the antenna to generate the desired far-field pattern [47]. The second alternative appears more practical and allows for diverse beamforming without modifying the antenna or to modify characteristics of already deployed antenna units.

In this context, we explore the realization of an all-dielectric Huygens' metasurface in the 120 GHz, and to use them for engineering the near-field distribution of diffusion-bonded planar slot array antennas for far-field beamforming. We use a laser drilling process to realize bridge-connected dielectric resonators that provide accurate prototyping of small resonator dimensions with no mechanical vibrations, thereby exhibiting very low fabrication tolerances. Laser drilling enables a single layer realization of all-dielectric structures in the 120 GHz band, whereby a single bridge is sufficient using a single layer dielectric only. We experimentally demonstrate these all-dielectric structures which are co-designed with planar slot array antennas, using them as transmit-arrays with beamforming capabilities. We further note that this is the first implementation of a Huygens' metasurface at these frequencies beyond 120 GHz, where the latest Huygens metasurfaces have been demonstrated up to 83 GHz only based on multi-layer metallic configuration [52], [53].

The paper is organized as follows. Sec. II presents the proposed Huygens' unit cell using full-wave driven-mode simulation to demonstrate the Huygens' resonances and the typical EM performance. Sec. II further compares the performance of the proposed all-dielectric unit cell with a metallic unit cell based on metallic patch resonators. Sec. III presents a full-wave demonstration of the transmit-array by operating in the near-field of a directive slot-array antenna to generate difference-pattern beams, as an illustrative example. Sec. IV presents an experimental demonstration of a uniform transmit-array to characterize its performance. A phase-gradient transmit-array is next demonstrated using beam-tilting as an example that can be achieved using the proposed structure. Conclusions are finally provided in Sec. V.

II. PROPOSED ALL-DIELECTRIC HUYGENS' STRUCTURE

A. HUYGENS' UNIT CELL

The proposed all-dielectric Huygens' unit cell is shown in Fig. 1(a). The unit cell is a dielectric shell disk with two interconnecting bridges to its neighboring disks. The presence of the bridges restricts the operation of the unit cell to polarizations orthogonal to the bridges ($y-$ polarized waves in this illustration). This unit cell was implemented at 60 GHz with machine drilling [54] but had poor performance due to mechanical vibrations when increased fabrication errors leading to inaccurate designs. A solution to the mechanical instability was recently proposed by using a dielectric unit cell with four interconnects, but this required an additional dielectric layer to cancel reflections from the extra interconnects, leading to a bulky design [47].

Here we propose using laser-drilling instead of mechanical drilling, which has not been explored for all-dielectric metasurfaces at these frequencies. Laser-drilling uses high precision laser beams, and the process is free from any mechanical vibrations. Consequently, it leads to high accuracy in the fabricated design which is paramount for high performance beamforming at high frequencies.

Finite-Element-Method (FEM) High Frequency Structure Simulator (HFSS) was used to demonstrate the EM performance of the unit cell. Fig. 1(b) shows the typical reflection and transmission response with a normally impinging plane waves (i.e. plane wave propagating in the $z-$ direction and polarizing in the $y-$direction). Two nulls are observed in the reflection plot, which correspond to zero back-scattering. These two frequencies (120.2 and 126.6 GHz) are the

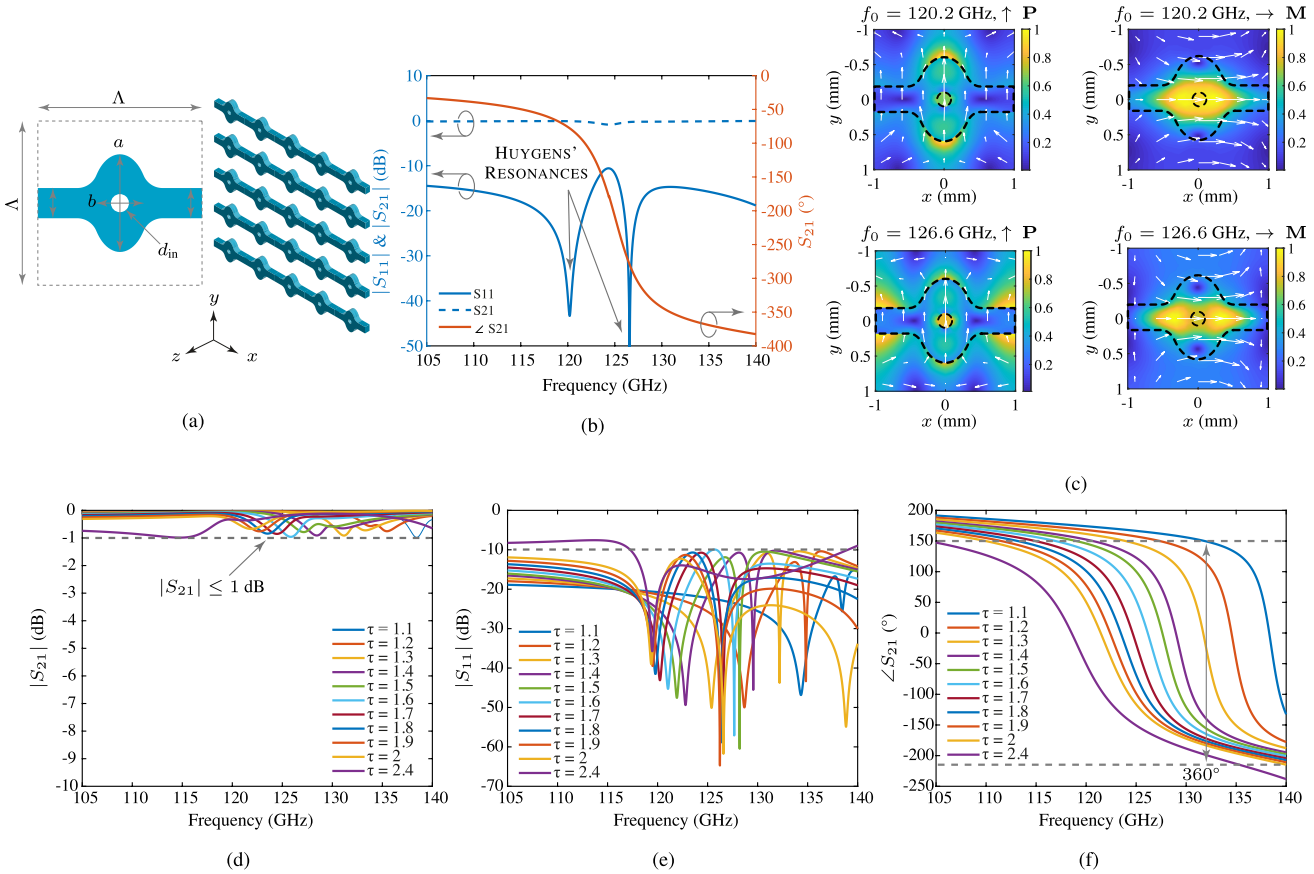

FIGURE 1. a) Proposed Huygens' transmit-array implemented on Rogers' RO3006 ($\epsilon_r = 6.5$, $\tan\delta = 0.0020$, $h = 25$ mil $= 0.635$ mm), $\Lambda = 2$ mm. Full-wave demonstration of Huygens' resonance using b) S-parameters and c) driven-mode fields at 120.2 and 126.6 GHz, showing orthogonal electric and magnetic dipoles. Dimensions of the unit cell used for this demonstration are $\Lambda = 2$ mm, $d_{in} = 0.22$ mm, $w = 0.37$ mm, and $a/b = \tau = 1.7$. Full-wave demonstration of various unit cells with varying ellipticities: d) transmission magnitude with loss < 1 dB for all unit cells, e) reflection magnitude showing wideband matching, and f) transmission phase showing full 360° phase variation achieved.

Huygens' resonances where the electric and magnetic dipoles are excited [19].

To demonstrate the Huygens' resonances, the driven-mode field plots are shown in Fig. 1(c) at 120.2 and 126.6 GHz. The field plots clearly show the electric field ($y-$axis) and magnetic field ($x-$axis) excited in the unit cell at both frequencies. The two fields are orthogonal, co-located, and occur at the same frequency, hence the Huygens' condition is met.

The dimensions of the unit cell were then varied to demonstrate the full 360° phase variation achieved with low reflection. The ratio a/b or ellipticity, τ, of the unit cell is the main dimension that controls the transmission phase. The diameter of the inner hole, d_{in} and the bridge widths, w, were used to optimize the performance for low reflection. Fig. 1(d) shows the transmission magnitude where the transmission loss is maintained below 1 dB across the bandwidth. Fig. 1(e) shows the reflection magnitude, where it is below -10 dB in a wide bandwidth from about 117 to 139 GHz. Finally, Fig. 1(f) shows the transmission phase for each unit cell, whereby varying the ellipticity a full 360° phase variation can be achieved.

B. ALL-DIELECTRIC VS METALLIC CELL

Next, the proposed all-dielectric structure will be compared with a metallic unit cell [46] as shown in Fig. 2(a). The metallic-PCB unit cell consists of two metallic patch resonators on either side of a dielectric substrate. The outer and inner ellipticity of the patch resonators are degrees of freedom to control the transmission phase while achieving good matching. Fig. 2(b) & (c) show the reflection and transmission magnitudes, respectively. Fig. 2(d) & (e) further show the transmission phase and the group delay, respectively.

The metallic and all-dielectric unit cells have comparable loss performance at the Huygens' resonances around 130 GHz. The all-dielectric cell however offers larger matching bandwidth and better transmission efficiency compared to the metallic one. Moreover, the all-dielectric cell features greater phase variation with frequency, which is also reflected in the larger transmission group delay response, as shown in Fig. 2(e). Besides, in terms of fabrication, the metallic unit cell is more challenging to fabricate at 120 GHz due to the high tolerance on the PCB fabrication requiring very small line-width of the elliptical resonator. Hence, the laser-drilled

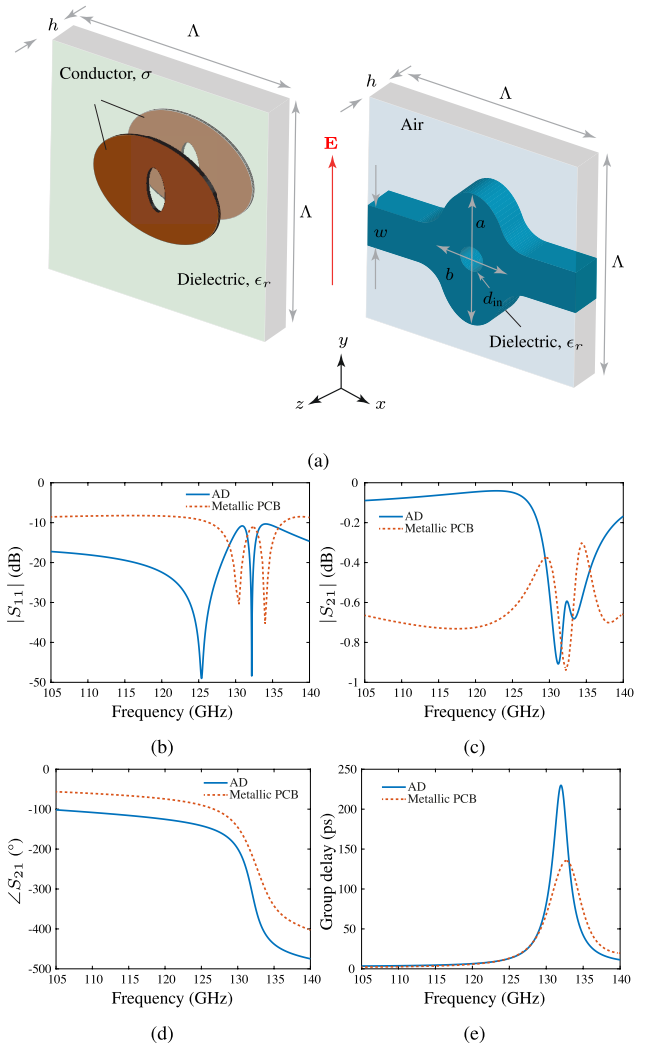

FIGURE 2. Comparison between a metallic-PCB unit cell [46] and the proposed all-dielectric unit cell. a) Illustration of the metallic-PCB unit cell based on metallic patch resonators and the proposed all-dielectric unit cell. The metallic-PCB unit cell was implemented using a substrate with the following properties: $\epsilon_r = 2$, $\tan\delta = 0.0021$, $h = 0.184$ mm, copper conductivity, $\sigma = 5.8 \times 10^7$ S/m, and has the following dimensions: $\Lambda = 2$ mm, elliptical patch outer ellipticity, $\tau_{\text{out}} = 1.5$, inner ellipticity (i.e. hole), $\tau_{\text{in}} = 0.5$, and copper thickness, $t = 15$ μm. The all-dielectric unit cell was implemented on Rogers' RO3006 ($\epsilon_r = 6.5$, $\tan\delta = 0.0020$, $h = 25$ mil $= 0.635$ mm), and has the following dimensions: $a/b = \tau = 2$, $w = 0.37$ mm, and $d_{\text{in}} = 0.22$ mm. Simulation results were obtained by exciting both unit cells with a normally impinging plane-wave to obtain b) reflection, transmission c) magnitude and d) phase, and e) group delay.

all-dielectric unit cell is an attractive solution to implement Huygens' surfaces above 100 GHz.

III. FULL-WAVE TRANSMIT-ARRAY DEMONSTRATION

A. HUYGENS' TRANSMIT-ARRAY ELEMENT

The proposed Huygens' unit cell will be used to engineer the near-field of a directive slot array antenna operating in the 120-GHz-band [55]. Fig. 3 shows the FEM-HFSS model of the *Huygens' element* consisting of one slot sub-array unit cell and four Huygens' unit cells. The distance between the top of

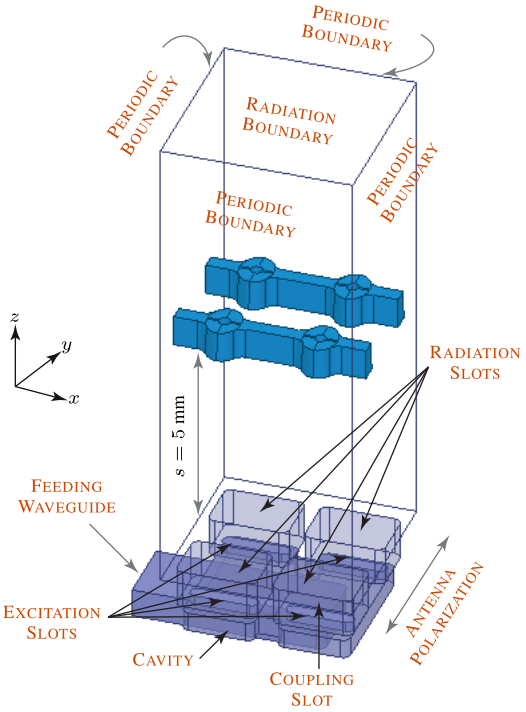

FIGURE 3. FEM-HFSS model of the Huygens' transmit-array element which consists of a slot array antenna unit cell and four Huygens' unit cells.

the antenna unit cell and the Huygens' unit cell is $s = 5$ mm, which was found to give an optimum matching performance. By repeating this composite slot sub-array and Huygens cell in 2D, the near-field phase may be spatially engineered. The proposed Huygens' surface thus acts a *transmit-array*.

The slot sub-array unit cell consists of a feeding waveguide which carries the power to a cavity. The coupling slots couples the power to the four slots which subsequently excite four radiation slots with linear polarization. The transmit-array is designed such that one unit cell covers one radiation slot, so that the slot array period fixes the transmit-arrays periodicity. The polarization of the antenna is the in $y-$direction (i.e. perpendicular to the Huygens' unit cell bridges). The antenna is designed with a uniform near-field phase, hence the Huygens' unit cell simulated with a normally impinging plane wave can be directly used with the antenna unit cell without any modification.

B. TRANSMIT-ARRAY BEAMFORMING

Full-wave simulations are next used to demonstrate the operation of the transmit-array on top of the slot array antenna. As an example of beamforming, a transmit-array was designed to achieve difference-pattern beams from one directive beam. Such a surface has one-half of the unit cell with a certain transmission phase, ϕ and the other half are out of phase (i.e. $\phi \pm 180$). When a wave is incident on a difference-pattern surface, a null will be created at the point of phase change due to the destructive interference of the fields. The null will cause the main beam of a directive antenna

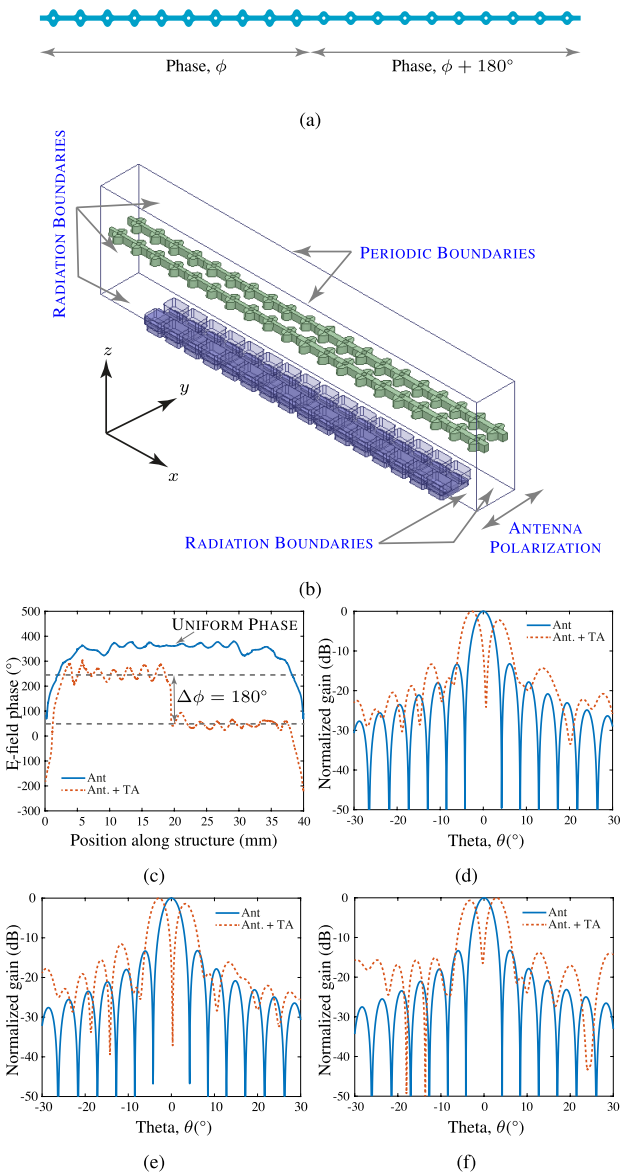

FIGURE 4. Full-wave demonstration of a difference-pattern transmit-array operating in the near-field of the slot array antenna. a) Illustration of 1-D array of the difference-pattern transmit-array. The unit cell with phase ϕ has dimensions: $\tau = 1.8$, $w = 0.46$ mm, and $d_{in} = 0.40$ mm, and the unit cell with phase $\phi + 180°$ has dimensions: $\tau = 1.4$, $w = 0.30$ mm, and $d_{in} = 0.40$ mm. b) FEM-HFSS model of the antenna and the transmit-array with boundary conditions. The separation between the top of the antenna and the bottom of the transmit-array is $s = 5$ mm. Simulation results of c) the near E-field phase at 126 GHz at 8 mm above the antenna, and H-plane far-field radiation pattern at d) 126 GHz, e) 127 GHz, and f) 128 GHz.

to split into two beams (i.e. difference-pattern beams). One application of difference-pattern transmit-array increasing the spatial coverage of directive antennas by splitting the main beam into two beams as was demonstrated in [47].

Fig. 4(a) shows an illustration of a 1-D array of the difference pattern structure. Fig. 4(b) shows the FEM-HFSS model of a 1-D array of the slot array unit cell and the difference-pattern structure. The phase variation was imposed in the H-plane of the antenna for best performance, which can be attributed to weak coupling between the slots in the H-plane. Periodic boundaries are used to achieve the full size of the array needed, which in this case is a 20 × 20 array of the transmit-array and an 8 × 8 array of the slot antenna unit cell (total 16 × 16 slots). Extra unit cells of the transmit-array are added around the antenna to reduce edge effects.

Fig. 4(c) shows the near E-field phase at 126 GHz and at 8 mm above the antenna with and without the difference-pattern transmit array. As can be seen, the antenna has a near-uniform phase distribution, and when the transmit-array is added the desired phase discontinuity of 180° is achieved. Fig. 4(d) and (e) further show the far-field radiation patterns of the antenna with and without the transmit-array at 126, 127, and 128 GHz. It is demonstrated that the transmit-array causes the main antenna beam at 0° to split into two beams, as desired.

Next, experimental demonstration of the proposed Huygens' transmit-array will be presented for uniform and phase-gradient transmit-arrays.

TABLE 1. Laser drilling machine specifications.

Specification	Value
Wavelength	515 nm
Pulse width	8 ps
Average output power	30 W
Maximum oscillation frequency	200 kHz
Beam size	10 µm
Focal length	163 mm or 100 mm
Taper angle	2.25°
Maximum scan speed	1500 mm/s (focal length 163 mm) 1000 mm/s (focal length 100 mm)
Position accuracy	15 µm (focal length 163 mm) 10 µm (focal length 100 mm)

IV. EXPERIMENTAL DEMONSTRATION

A. LASER-DRILLING PROCESS AND SPECIFICATIONS

Laser-drilling is the process of using focused high energy laser beams to cut, drill, or mill a material. In the process, the material is removed by a combination of melting and evaporation [56]. It provides high accuracy, fast drilling rates, and is capable of drilling smaller hole sizes than standard PCB fabrication [57]. Table 1 shows the specifications of the laser-drilling process used to fabricate the proposed design. The most important parameter that influences the design stage is the taper angle of the laser beam. For best accuracy and agreement with simulation, a taper angle of 2.25° from the top to the bottom of the substrate was taken into consideration in the FEM-HFSS designs.

To investigate the effect of the transmit-array on the antenna and the accuracy of the laser drilling process, a uniform structure was first fabricated, where the same unit cell was used throughout the array. Fig. 5(a) & (b) show the slot array antenna and the uniform transmit-array,

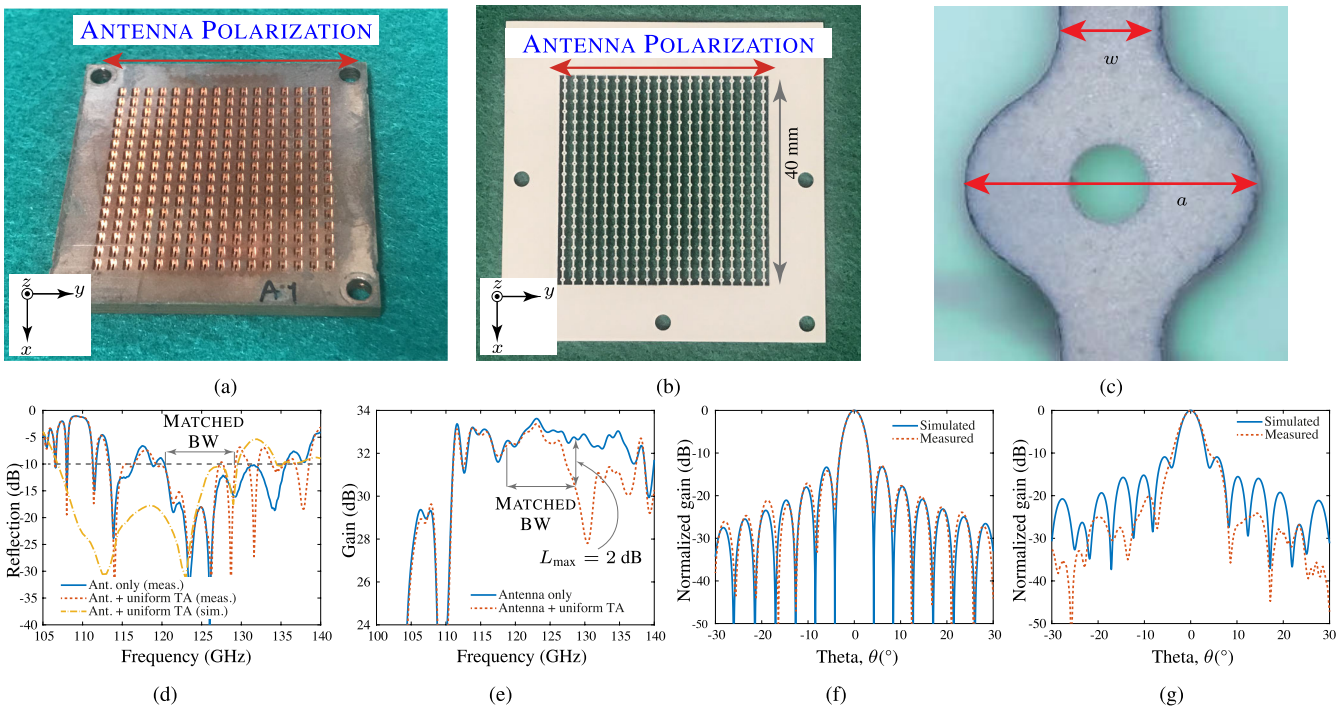

FIGURE 5. Experimental demonstration of a uniform transmit-array. a) Slot array antenna. b) Fabricated uniform transmit-array with unit cell dimensions: $\tau = 1.3$, $w = 0.322$ mm, and $d_{in} = 0.22$ mm. c) Photo of the unit cell under the microscope for dimension measurements. Measured antenna and uniform transmit-array performance: d) reflection measurements of the antenna only and the antenna with the uniform transmit-array, e) gain versus frequency of antenna only and antenna with uniform transmit-array, measured versus simulated H-plane far-field radiation pattern at 128 GHz for f) antenna only, and g) antenna with transmit-array. The separation between the antenna and the transmit-array is $s = 5$ mm.

respectively. To verify fabrication accuracy, the unit cells were measured under the microscope as shown in Fig. 5(c). Table 2 shows the design, average measured, and standard deviation for two dimensions, a and w. Dimension a has an average error of 9 μm with a standard deviation of 13 μm, while dimension w has an average error of 2 μm with a standard deviation of 14 μm. These errors are within the position accuracy of 10 to 15 μm shown in Table 1, and thus represent very low dimensional tolerances along with excellent repeatability.

The antenna reflection and far-field radiation characteristics were first measured. The transmit-array was then placed on top of the antenna with plastic washers in between to get a separation of 5 mm, and fastened using four plastic screws in the corners. The antenna together with the transmit-array was then measured. Fig. 5(d) shows the measured reflection of the antenna only, and the antenna with the transmit-array in measurements and simulation. Generally, the transmit-array has negligible effect on the reflection except above about 128 GHz, which was also predicted by full-wave simulations. The -10 dB matching bandwidth of the antenna and the transmit array is from 119 to 128 GHz.

Fig. 5(e) shows the measured gain of the antenna only and the antenna with the transmit-array. In the matched bandwidth of 119 to 128 GHz, it is shown that transmit-array causes has a maximum gain drop of 2 dB at 128 GHz, which is indicative of its dissipation losses. Fig. 5(f) shows the far-field radiation pattern of the antenna in measurements and simulation, showing almost identical performance, which indicates a good phase uniformity across the surface and fabrication robustness. Fig. 5(g) further shows the far-field radiation pattern of the antenna with the transmit-array in measurements and simulations, where the shape is comparable around the main lobe.

B. PHASE-GRADIENT TRANSMIT-ARRAY

Next, a phase-gradient transmit-array was fabricated to experimentally demonstrate beam-tilting as an example of beamforming using the proposed Huygens' unit cell. To achieve beam-titling from the antenna, a phase-gradient from 0 to 360° must be imposed in the near-field within a given spatial distance, which can be achieved using unit cells of the proposed Huygens' cells with varying ellipticities as shown in Fig. 1(f).

Fig. 6(a) shows a 1-D array of the phase-gradient transmit-array where the ellipticity decreases and phase increases from left to right. The phase-gradient transmit-array was placed on top of the slot array antenna and then near-field phase at 129 GHz is shown in Fig. 6(b). It is shown that a phase-gradient, $k_{x0} = 2\pi/32$ mm $= 196$ rad/m is achieved. The beam-tilt angle achieved using this phase-gradient can be calculated using

$$\theta(\omega) = \sin^{-1}\left(\frac{k_{x0}}{k_0}\right) \tag{1}$$

where k_0 is the free-space phase constant.

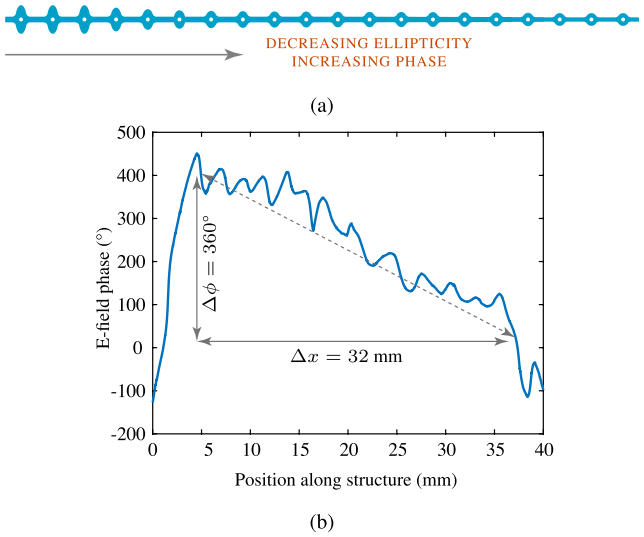

FIGURE 6. **Full-wave demonstration of the near-field of the slot array antenna with a phase-gradient transmit-array. a) 1-D array illustration of the phase-gradient transmit-array, and b) near E-field phase at 129 GHz at 8 mm from the top of the antenna.**

Fig. 7(a) shows the fabricated phase-gradient transmit-array. To verify fabrication accuracy, three unit cells were selected and measured under a microscope as shown in Fig. 7(b). Table 2 shows the design, average, and standard deviations of the dimensions a and w. Just like the uniform transmit-array, high fabrication accuracy is achieved. The reflection of the antenna with the phase-gradient was then measured as shown in Fig. 7(c). Reflection below -10 dB is obtained from 120 to 132 GHz. Fig. 7(d)-(e) show the measured far-field radiation patterns of the antenna with the transmit-array at 128, 129 and 130 GHz, where a clear beam-tilt is observed at each frequency, comparable with the simulation results.

The theoretical tilt angles can be calculated at 128, 129, and 130 GHz as follows: $\theta_{128\,\mathrm{GHz}} = \sin^{-1}(k_{x0}/k_{0,128\,\mathrm{GHz}}) = 4.20°$, $\theta_{129\,\mathrm{GHz}} = \sin^{-1}(k_{x0}/k_{0,129\,\mathrm{GHz}}) = 4.17°$, and $\theta_{130\,\mathrm{GHz}} = \sin^{-1}(k_{x0}/k_{0,130\,\mathrm{GHz}}) = 4.14°$. Comparable tilt angles were achieved in measurements: $\theta_{128\,\mathrm{GHz,\,meas.}} = 5°$, $\theta_{129\,\mathrm{GHz,\,meas.}} = 4.2°$, and $\theta_{130\,\mathrm{GHz,\,meas.}} = 4°$. Note that the side-lobe levels (SLL) are high (≈ -4 dB) in both simulations and measurements, as shown in Fig. 7(d)-(f). One of the reasons for the high SLL is spurious diffraction orders which occur due to the simple design of the phase-gradient transmit-array [58]. In addition, the large unit cell size also leads to poor discretization of the phase-gradient, as shown in Fig. 6(b). In the proposed design, the Huygens' unit cell size was restricted to 2×2 mm to match the size of the slot array antenna unit cell. To reduce the SLL, the phase discretization can be improved by making the unit cell smaller using a higher permittivity dielectric, for instance [47]. Furthermore, from a more theoretical point of view, the side-lobes can completely be eliminated by using a bianisotropic unit cell to suppress spurious diffraction orders, which has been demonstrated in [58] for example, using a three-layer metallic bianisotropic unit cell. Therefore a complete elimination of the side-lobes will require devising a

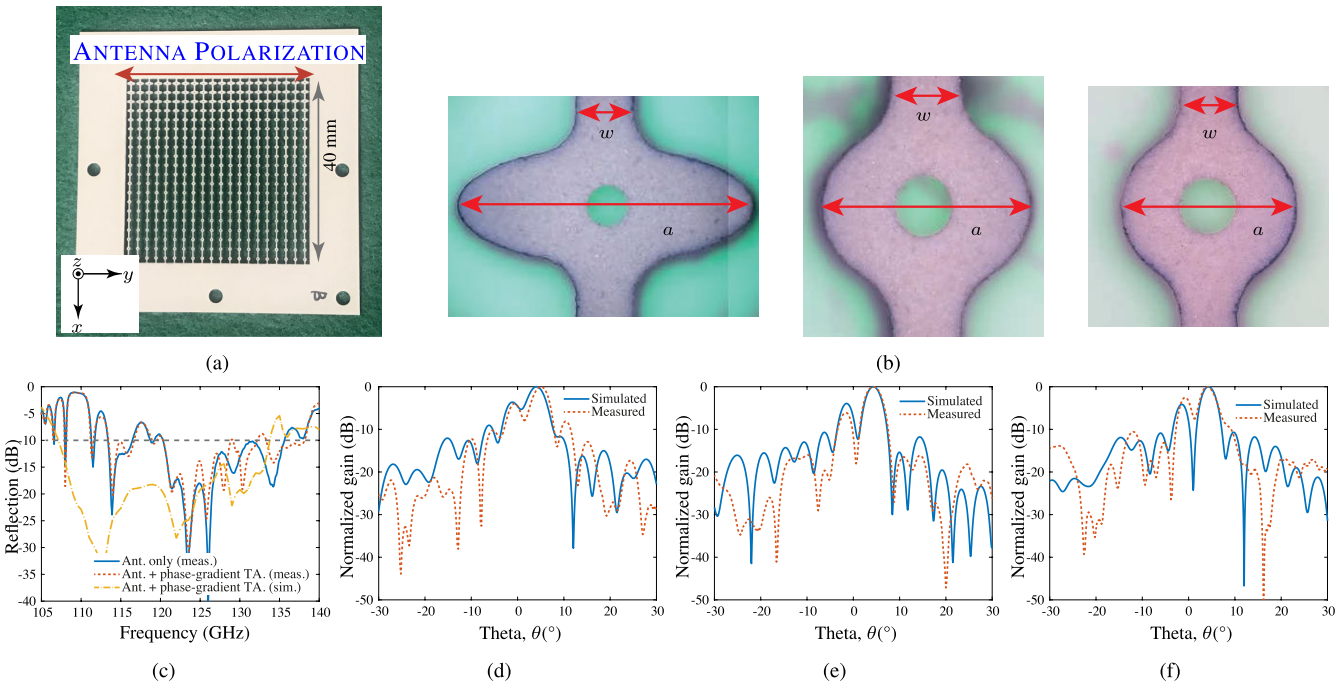

FIGURE 7. **Experimental demonstration of a phase-gradient transmit-array. a) Fabricated phase-gradient transmit-array. b) Photos of three selected unit cells under the microscope for dimension measurements. Measured antenna and the phase-gradient transmit-array performance: c) reflection measurements of the antenna only and the antenna with the phase-gradient transmit-array, and measured versus simulated H-plane far-field radiation patterns at b) 128 GHz, c) 129 GHz, d) 130 GHz.**

TABLE 2. Microscope measurements of the uniform transmit-array unit cell and three selected unit cells of the phase-gradient transmit-array.

	Uniform unit cell		Phase-gradient unit cell 1		Phase-gradient unit cell 2		Phase-gradient unit cell 3	
	a (mm)	w (mm)	a (mm)	w (mm)	a (mm)	w (mm)	a (mm)	w (mm)
Design	0.937	0.322	1.785	0.332	0.937	0.322	0.777	0.244
Average measured	0.928	0.320	1.788	0.342	0.917	0.296	0.781	0.256
Deviation	0.013	0.014	0.005	0.009	0.013	0.009	0.004	0.007

TABLE 3. Comparison between the proposed structure and microwave Huygens' metasurface (HMS) designs in literature.

Ref.	HMS Type	Fabrication Technique	Number of Layers	Frequency	Application
[59]	Metallic	Standard PCB process	4	10 GHz	Beam-focusing
[60]		Standard PCB process	4	9.4 to 10.6 GHz	Beam-focusing
[61]		Standard PCB process	6	5.6 & 15 GHz	Beam-focusing
[62]		Standard PCB process	2	20 GHz	Beam-tilting
[19]		Standard PCB process	2	24 to 28 GHz	Lens
[46]		Standard PCB process	2	58 to 63 GHz	Beam-tilting, splitting & lens
[52]		Standard PCB process	3	83 GHz	Lens
[53]		Standard PCB process	3	83 GHz	Beam-tilting
[63]	All-dielectric	CNC-machining	3	9 to 11 GHz	Beam-tilting
[47]		CNC-machining	2	58 to 62 GHz	Beam-tilting & splitting
This work		Laser-drilling	1	120 to 130 GHz	Beam-tilting

more complex all-dielectric unit cell exhibiting bianisotropy, compared to the simple one used here in this work.

The discrepancies between measurement and simulation results can be due to various factors. First, the dielectric constant and the loss tangent of the substrate are not known at the design frequencies, where even a small deviation from the design values can cause significant variation between simulation and measurements. In addition, it was assumed the substrate properties were constant with frequencies, which may not have been the case, especially considering the high frequency of operation of the proposed designs. Another issue is misalignment between the antenna and the transmit-array structure. The antenna/transmit-array structure was simulated under ideal alignment and flatness conditions, hence any deviation from that will cause significant impact on the measurements. In spite of these unknown factors, the transmit-array provides a good performance.

V. CONCLUSION

In this paper, a novel laser-drilled all-dielectric Huygens' transmit-array was proposed and experimentally demonstrated in the 120-GHz-band by operating in the near-field of a slot array antenna. The proposed structure is an array of dielectric shell disks connected with neighboring disks with dielectric bridges. The all-dielectric unit cell was demonstrated to excite Huygens' resonances hence achieving EM wave transformations with zero back-scattering. The proposed unit cell was compared with a metallic unit cell based on metallic patch resonators, and it exhibits comparable loss performance, with the added advantage of fabrication accuracy achieved using laser-drilling. A uniform array of the proposed unit was first fabricated to characterize its effect on the antenna gain and estimate the fabrication tolerance using the laser drilling process. It was found to cause a maximum drop in gain of about 2 dB. A phase-gradient transmit-array was then fabricated to successfully demonstrate beam-titling as an example of beam-forming in the 120-GHz-band. Table 3 finally shows a comparison between the proposed structure and other Huygens' metasurface (HMS) designs at microwave frequencies, including metallic PCB-based as well as all-dielectric metasurfaces. The majority of metasurface designs in literature consist of two or more metallic layers on a dielectric and are fabricated using the standard PCB process [19], [46], [59]–[62]. On the other hand, all-dielectric designs at microwave frequencies are typically fabricated using CNC-machining [47], [63], with the proposed design being the first of its kind that uses laser-drilling to achieve high-precision fabrication. The proposed laser drilled all-dielectric Huygens' transmit-array may thus represent an attractive alternate to a standard PCB based fabrication for passive antenna beam-forming above 100-GHz for beyond 5G communication networks.

ACKNOWLEDGMENT

The authors would like to acknowledge L.P.S. Works Company Ltd., (Suite 409, Ota Techno Core, 6-4-17 Higashikojiya, Ota-ku, Tokyo 144-0033) for the fabrication of the transmit-arrays.

REFERENCES

[1] C. L. Holloway, E. F. Kuester, J. A. Gordon, J. O'Hara, J. Booth, and D. R. Smith, "An overview of the theory and applications of metasurfaces: The two-dimensional equivalents of metamaterials," *IEEE Antennas Propag. Mag.*, vol. 54, no. 2, pp. 10–35, Apr. 2012.

[2] M. K. T. Al-Nuaimi, W. Hong, and W. G. Whittow, "Aperiodic sunflower like metasurface for diffusive scattering and RCS reduction," *IEEE Antennas Wireless Propag. Lett.*, vol. 19, no. 7, pp. 1048–1052, Jul. 2020.

[3] A. M. H. Wong and G. V. Eleftheriades, "Perfect anomalous reflection with a bipartite Huygens' metasurface," *Phys. Rev. X*, vol. 8, no. 1, Feb. 2018, Art. no. 011036.

[4] P. Moitra, B. A. Slovick, Z. Gang Yu, S. Krishnamurthy, and J. Valentine, "Experimental demonstration of a broadband all-dielectric metamaterial perfect reflector," *Appl. Phys. Lett.*, vol. 104, no. 17, Apr. 2014, Art. no. 171102.

[5] X. Huang, H. Yang, D. Zhang, and Y. Luo, "Ultrathin dual-band metasurface polarization converter," *IEEE Trans. Antennas Propag.*, vol. 67, no. 7, pp. 4636–4641, Jul. 2019.

[6] B. Lin, L. Lv, J. Guo, Z. Liu, X. Ji, and J. Wu, "An ultra-wideband reflective Linear-to-Circular polarization converter based on anisotropic metasurface," *IEEE Access*, vol. 8, pp. 82732–82740, 2020.

[7] A. Arbabi, Y. Horie, M. Bagheri, and A. Faraon, "Dielectric metasurfaces for complete control of phase and polarization with subwavelength spatial resolution and high transmission," *Nature Nanotechnol.*, vol. 10, no. 11, pp. 937–943, Nov. 2015.

[8] K. Achouri, B. A. Khan, S. Gupta, G. Lavigne, M. A. Salem, and C. Caloz, "Synthesis of electromagnetic metasurfaces: Principles and illustrations," *EPJ Appl. Metamaterials*, vol. 2, p. 12, Oct. 2015.

[9] N. M. Estakhri and A. Alù, "Recent progress in gradient metasurfaces," *J. Opt. Soc. Amer. B, Opt. Phys.*, vol. 33, no. 2, pp. A21–A30, Feb. 2016.

[10] C. R. de Galarreta, A. Alexeev, J. Bertolotti, and C. D. Wright, "Phase-change metasurfaces for dyamic beam steering and beam shaping in the infrared," in *Proc. IEEE Int. Symp. Circuits Syst. (ISCAS)*, May 2018, pp. 1–5.

[11] N. I. Landy, S. Sajuyigbe, J. J. Mock, D. R. Smith, and W. J. Padilla, "Perfect metamaterial absorber," *Phys. Rev. Lett.*, vol. 100, May 2008, Art. no. 207402.

[12] K. V. Sreekanth, M. ElKabbash, Y. Alapan, A. R. Rashed, U. A. Gurkan, and G. Strangi, "A multiband perfect absorber based on hyperbolic metamaterials," *Sci. Rep.*, vol. 6, no. 1, Sep. 2016, Art. no. 26272.

[13] Y. Ra'di, V. S. Asadchy, and S. A. Tretyakov, "Total absorption of electromagnetic waves in ultimately thin layers," *IEEE Trans. Antennas Propag.*, vol. 61, no. 9, pp. 4606–4614, Sep. 2013.

[14] R. Wang, B.-Z. Wang, Z.-S. Gong, and X. Ding, "Creation of an arbitrary electromagnetic illusion using a planar ultrathin metasurface," *IEEE Photon. J.*, vol. 9, no. 4, pp. 1–9, Aug. 2017.

[15] M. Gharghi, C. Gladden, T. Zentgraf, Y. Liu, X. Yin, J. Valentine, and X. Zhang, "A carpet cloak for visible light," *Nano Lett.*, vol. 11, no. 7, pp. 2825–2828, Jul. 2011.

[16] M. Chen, M. Kim, A. M. H. Wong, and G. V. Eleftheriades, "Huygens' metasurfaces from microwaves to optics: A review," *Nanophotonics*, vol. 7, no. 6, pp. 1207–1231, Jun. 2018.

[17] M. Decker, I. Staude, M. Falkner, J. Dominguez, D. N. Neshev, I. Brener, T. Pertsch, and Y. S. Kivshar, "High-efficiency dielectric Huygens' surfaces," *Adv. Opt. Mater.*, vol. 3, no. 6, pp. 813–820, 2015.

[18] M. Kim, A. M. H. Wong, and G. V. Eleftheriades, "Optical Huygens' metasurfaces with independent control of the magnitude and phase of the local reflection coefficients," *Phys. Rev. X*, vol. 4, no. 4, Dec. 2014, Art. no. 041042.

[19] C. Xue, Q. Lou, and Z. N. Chen, "Broadband double-layered Huygens' metasurface lens antenna for 5G millimeter-wave systems," *IEEE Trans. Antennas Propag.*, vol. 68, no. 3, pp. 1468–1476, Mar. 2020.

[20] H. C. Chou, N.-L. Tung, and M. N. M. Kehn, "The double-focus generalized Luneburg lens design and synthesis using metasurfaces," *IEEE Trans. Antennas Propag.*, vol. 66, no. 9, pp. 4936–4941, Sep. 2018.

[21] J. D. Ortiz, J. D. Baena, V. Losada, F. Medina, R. Marqués, and J. L. A. Quijano, "Self-complementary metasurface for designing narrow band pass/stop filters," *IEEE Microw. Wireless Compon. Lett.*, vol. 23, no. 6, pp. 291–293, Jun. 2013.

[22] C. Ni, M. S. Chen, Z. X. Zhang, and X. L. Wu, "Design of frequency-and polarization-reconfigurable antenna based on the polarization conversion metasurface," *IEEE Antennas Wireless Propag. Lett.*, vol. 17, no. 1, pp. 78–81, Jan. 2018.

[23] X. Liu, J. Zhang, W. Li, R. Lu, L. Li, Z. Xu, and A. Zhang, "Three-band polarization converter based on reflective metasurface," *IEEE Antennas Wireless Propag. Lett.*, vol. 16, pp. 924–927, 2017.

[24] F. Qin, L. Wan, L. Li, H. Zhang, G. Wei, and S. Gao, "A transmission metasurface for generating OAM beams," *IEEE Antennas Wireless Propag. Lett.*, vol. 17, no. 10, pp. 1793–1796, Oct. 2018.

[25] D. J. Gregoire, "3-D conformal metasurfaces," *IEEE Antennas Wireless Propag. Lett.*, vol. 12, pp. 233–236, 2013.

[26] N. Muhammad, Z. Ouyang, X. Tang, and Q. Liu, "Broadband wide-angle incident light absorption by metallic loop metasurfaces based on electro-optic substrate," *IEEE Photon. Technol. Lett.*, vol. 31, no. 13, pp. 1068–1071, Jul. 1, 2019.

[27] X. Hu and X. Wei, "Metallic metasurface for high efficiency optical phase control in transmission mode," *Opt. Express*, vol. 25, no. 13, pp. 15208–15215, Jun. 2017.

[28] K. Achouri, A. Yahyaoui, S. Gupta, H. Rmili, and C. Caloz, "Dielectric resonator metasurface for dispersion engineering," *IEEE Trans. Antennas Propag.*, vol. 65, no. 2, pp. 673–680, Feb. 2017.

[29] J. L. Wu, Y. M. Pan, W. Che, and G.-L. Huang, "Design of high-transmittance all-dielectric focusing metasurface with polarization-controllable focus," *IEEE Trans. Antennas Propag.*, vol. 68, no. 8, pp. 6183–6192, Aug. 2020.

[30] M. K. T. Al-Nuaimi, Y. He, and W. Hong, "Design of inhomogeneous all-dielectric electromagnetic-wave diffusive reflectarray metasurface," *IEEE Antennas Wireless Propag. Lett.*, vol. 18, no. 4, pp. 732–736, Apr. 2019.

[31] L. Shao, M. Premaratne, and W. Zhu, "Dual-functional coding metasurfaces made of anisotropic all-dielectric resonators," *IEEE Access*, vol. 7, pp. 45716–45722, 2019.

[32] J. Diao, B. Han, J. Yin, X. Li, T. Lang, and Z. Hong, "Analogue of electromagnetically induced transparency in an S-Shaped all-dielectric metasurface," *IEEE Photon. J.*, vol. 11, no. 3, pp. 1–10, Jun. 2019.

[33] V. M. Pepino, A. F. da Mota, A. Martins, and B.-H.-V. Borges, "3-D-Printed dielectric metasurfaces for antenna gain improvement in the ka-band," *IEEE Antennas Wireless Propag. Lett.*, vol. 17, no. 11, pp. 2133–2136, Nov. 2018.

[34] C. Yang, Z. Wang, H. Yuan, K. Li, X. Zheng, W. Mu, W. Yuan, Y. Zhang, and W. Shen, "All-dielectric metasurface for highly tunable, narrowband notch filtering," *IEEE Photon. J.*, vol. 11, no. 4, pp. 1–6, Aug. 2019.

[35] B. Wang, F. Dong, Q.-T. Li, D. Yang, C. Sun, J. Chen, Z. Song, L. Xu, W. Chu, Y.-F. Xiao, Q. Gong, and Y. Li, "Visible-frequency dielectric metasurfaces for multiwavelength achromatic and highly dispersive holograms," *Nano Lett.*, vol. 16, no. 8, pp. 5235–5240, Aug. 2016.

[36] D. Lin, P. Fan, E. Hasman, and M. L. Brongersma, "Dielectric gradient metasurface optical elements," *Science*, vol. 345, no. 6194, pp. 298–302, Jul. 2014.

[37] Z. Lin, L. Huang, R. Zhao, Q. Wei, T. Zentgraf, Y. Wang, and X. Li, "Dynamic control of mode modulation and spatial multiplexing using hybrid metasurfaces," *Opt. Express*, vol. 27, no. 13, pp. 18740–18750, Jun. 2019.

[38] X. Zang, F. Dong, F. Yue, C. Zhang, L. Xu, Z. Song, M. Chen, P.-Y. Chen, G. S. Buller, Y. Zhu, S. Zhuang, W. Chu, S. Zhang, and X. Chen, "Polarization encoded color image embedded in a dielectric metasurface," *Adv. Mater.*, vol. 30, no. 21, May 2018, Art. no. 1707499.

[39] B. H. Chen, P. C. Wu, V.-C. Su, Y.-C. Lai, C. H. Chu, I. C. Lee, J.-W. Chen, Y. H. Chen, Y.-C. Lan, C.-H. Kuan, and D. P. Tsai, "GaN metalens for pixel-level full-color routing at visible light," *Nano Lett.*, vol. 17, no. 10, pp. 6345–6352, Oct. 2017.

[40] S. Gao, C.-S. Park, S.-S. Lee, and D.-Y. Choi, "All-dielectric metasurfaces for simultaneously realizing polarization rotation and wavefront shaping of visible light," *Nanoscale*, vol. 11, no. 9, pp. 4083–4090, 2019.

[41] A. Howes, W. Wang, I. Kravchenko, and J. Valentine, "Dynamic transmission control based on all-dielectric Huygens metasurfaces," *Optica*, vol. 5, no. 7, pp. 787–792, Jul. 2018.

[42] C. Liu, L. Chen, T. Wu, Y. Liu, J. Li, Y. Wang, Z. Yu, H. Ye, and L. Yu, "All-dielectric three-element transmissive Huygens' metasurface performing anomalous refraction," *Photon. Res.*, vol. 7, no. 12, pp. 1501–1510, Dec. 2019.

[43] S. Jahani and Z. Jacob, "All-dielectric metamaterials," *Nature Nanotechnol.*, vol. 11, no. 1, pp. 23–36, Jan. 2016.

[44] S. An, C. Fowler, M. Y. Shalaginov, Y. Zhang, P. Su, M. Kang, B. Zheng, H. Tang, H. Li, A. M. Agarwal, C. Rivero-Baleine, K. A. Richardson, T. Gu, J. Hu, and H. Zhang, "Modeling of all-dielectric metasurfaces using deep neural networks," in *Proc. Int. Appl. Comput. Electromagn. Soc. Symp. (ACES)*, 2019, pp. 1–2.

[45] A. Monti, A. Alu, A. Toscano, and F. Bilotti, "Surface impedance modeling of all-dielectric metasurfaces," *IEEE Trans. Antennas Propag.*, vol. 68, no. 3, pp. 1799–1811, Mar. 2020.

[46] S. Sakurai, J. G. N. Rahmeier, T. Tomura, J. Hirokawa, and S. Gupta, "Millimeter-wave Huygens' transmit-arrays based on coupled metallic resonators," 2020, *arXiv:2004.07129*. [Online]. Available: http://arxiv.org/abs/2004.07129

[47] M. K. Emara, T. Tomura, J. Hirokawa, and S. Gupta, "All-dielectric Fabry-Pérot based compound Huygens' structure for millimeter-wave beam-forming," *IEEE Trans. Antennas Propag.*, early access, Jul. 2, 2020, doi: 10.1109/TAP.2020.3005233.

[48] K. Maheshwari, "Investigation of all-dielectric Hugyens' metasurfaces at millimeter-wave frequencies," M.S. thesis, Dept. Electron., Carleton Univ., Ottawa, ON, Canada, 2019.

[49] T. S. Rappaport, Y. Xing, O. Kanhere, S. Ju, A. Madanayake, S. Mandal, A. Alkhateeb, and G. C. Trichopoulos, "Wireless communications and applications above 100 GHz: Opportunities and challenges for 6G and beyond," *IEEE Access*, vol. 7, pp. 78729–78757, 2019.
[50] M. K. Emara, T. Tomura, J. Hirokawa, and S. Gupta, "All-dielectric Huygens' metasurface pair for mm-Wave circularly-polarized beam-forming," in *Proc. 14th Eur. Conf. Antennas Propag. (EuCAP)*, Mar. 2020, pp. 1–4.
[51] M. Zhang, K. Toyosaki, J. Hirokawa, M. Ando, T. Taniguchi, and M. Noda, "A 60-GHz band compact-range gigabit wireless access system using large array antennas," *IEEE Trans. Antennas Propag.*, vol. 63, no. 8, pp. 3432–3440, Aug. 2015.
[52] A. E. Olk and D. A. Powell, "Huygens metasurface lens for W-Band switched beam antenna applications," *IEEE Open J. Antennas Propag.*, vol. 1, pp. 290–299, 2020.
[53] A. E. Olk, P. E. M. Macchi, and D. A. Powell, "High-efficiency refracting millimeter-wave metasurfaces," *IEEE Trans. Antennas Propag.*, vol. 68, no. 7, pp. 5453–5462, Jul. 2020.
[54] S. Gupta, T. Tomura, S. Sakurai, D. J. King, and J. Hirokawa, "Millimeter-wave Huygens' metasurfaces based on all-dielectric resonators for antenna beam-forming," in *Proc. 13th Eur. Conf. Antennas Propag. (EuCAP)*, 2019, pp. 1–3.
[55] D. Kim, J. Hirokawa, K. Sakurai, M. Ando, T. Takada, T. Nagatsuma, J. Takeuchi, and A. Hirata, "Design and measurement of the plate laminated waveguide slot array antenna and its feasibility for wireless link system in the 120 GHz band," *IEICE Trans. Commun.*, vol. E96.B, no. 8, pp. 2102–2111, 2013.
[56] C. M. Adams and G. A. Hardway, "Fundamentals of laser beam machining and drilling," *IEEE Trans. Ind. Gen. Appl.*, vol. IGA-1, no. 2, pp. 90–96, Mar. 1965.
[57] C. J. Moorhouse, F. J. Villarreal, H. J. Baker, and D. R. Hall, "Laser drilling of copper foils for electronics applications," *IEEE Trans. Compon. Packag. Technol.*, vol. 30, no. 2, pp. 254–263, Jun. 2007.
[58] G. Lavigne, K. Achouri, V. S. Asadchy, S. A. Tretyakov, and C. Caloz, "Susceptibility derivation and experimental demonstration of refracting metasurfaces without spurious diffraction," *IEEE Trans. Antennas Propag.*, vol. 66, no. 3, pp. 1321–1330, Mar. 2018.
[59] H. Li, G. Wang, H.-X. Xu, T. Cai, and J. Liang, "X-band phase-gradient metasurface for high-gain lens antenna application," *IEEE Trans. Antennas Propag.*, vol. 63, no. 11, pp. 5144–5149, Nov. 2015.
[60] J.-J. Liang, G.-L. Huang, J.-N. Zhao, Z.-J. Gao, and T. Yuan, "Wideband phase-gradient metasurface antenna with focused beams," *IEEE Access*, vol. 7, pp. 20767–20772, 2019.
[61] H. Yue, L. Chen, Y. Yang, L. He, and X. Shi, "Design and implementation of a dual frequency and bidirectional phase gradient metasurface for beam convergence," *IEEE Antennas Wireless Propag. Lett.*, vol. 18, no. 1, pp. 54–58, Jan. 2019.
[62] M. Chen and G. V. Eleftheriades, "Omega-bianisotropic wire-loop Huygens' metasurface for reflectionless wide-angle refraction," *IEEE Trans. Antennas Propag.*, vol. 68, no. 3, pp. 1477–1490, Mar. 2020.
[63] S. S. Bahramipour, K. Afrooz, M. M. Honari, R. Mirzavand, and P. Mousavi, "Gradient and Huygens' metasurface design and analysis based on transmission line theory," *IEEE Trans. Antennas Propag.*, early access, Apr. 10, 2020, doi: 10.1109/TAP.2020.2984908.

MOHAMED K. EMARA (Graduate Student Member, IEEE) received the B.Eng. degree in aerospace engineering and the M.A.Sc. degree in electrical and computer engineering from Carleton University, Ottawa, ON, Canada, in 2016 and 2018, respectively, where he is currently pursuing the Ph.D. degree in electrical and computer engineering with a focus on leaky-wave antennas (LWAs) and metasurfaces for electromagnetic wave control. His M.A.Sc. thesis was focused on dispersive electromagnetic structures for surface wave control on antenna ground planes and guided wave control in half-mode substrate integrated waveguides (HMSIWs) for analog-signal processing (ASP) applications.

He was a recipient of the Undergraduate Senate Medal for the Outstanding Academic Achievement in 2016, the Ontario Graduate Scholarship from 2016 to 2017 and from 2020 to 2021, the Natural Sciences and Engineering Research Council (NSERC) Alexander Graham Bell Canada Graduate Scholarship from 2020 to 2023, the Honorable Mention in the Student Paper Competition from the 2020 IEEE Antennas and Propagation Symposium (APS), and the Student Paper Competition Winner from the 2018 International Symposium on Antenna Technology and Applied Electromagnetics (ANTEM), Waterloo, ON, Canada.

SONYA K. STUHEC-LEONARD (Student Member, IEEE) received the B.Eng. degree in engineering physics from Carleton University, Ottawa, ON, Canada, in 2018, where she is currently pursuing the M.A.Sc. degree in metasurfaces for electromagnetic wave control with the Department of Electronics.

TAKASHI TOMURA (Member, IEEE) received the B.S., M.S., and D.E. degrees in electrical and electronic engineering from the Tokyo Institute of Technology, Tokyo, Japan, in 2008, 2011, and 2014, respectively.

He was a Research Fellow with the Japan Society for the Promotion of Science (JSPS) in 2013. From 2014 to 2017, he was with Mitsubishi Electric Corporation, Tokyo. He was engaged in research and development of aperture antennas for satellite communications and radar systems. From 2017 to 2019, he was a Specially Appointed Assistant Professor with the Tokyo Institute of Technology, where he is currently an Assistant Professor. His research interests include electromagnetic analysis, aperture antennas, and planar waveguide slot array antennas. He received the Best Student Award from Ericsson, Japan, in 2012, the IEEE AP-S Tokyo Chapter Young Engineer Award in 2015, and the Young Researcher Award from the IEICE Technical Committee on Antennas and Propagation in 2018. He is a member of IEICE.

JIRO HIROKAWA (Fellow, IEEE) received the B.S., M.S., and D.E. degrees in electrical and electronic engineering from the Tokyo Institute of Technology (Tokyo Tech), Tokyo, Japan, in 1988, 1990, and 1994, respectively.

He was a Research Associate from 1990 to 1996 and an Associate Professor from 1996 to 2015 with Tokyo Tech. He was with the Antenna Group, Chalmers University of Technology, Gothenburg, Sweden, as a Postdoctoral Fellow, from 1994 to 1995. He is currently a Professor with Tokyo Tech. His research interests include slotted waveguide array antennas and millimeter-wave antennas. He received the IEEE AP-S Tokyo Chapter Young Engineer Award in 1991, the Young Engineer Award from IEICE in 1996, the Tokyo Tech Award for Challenging Research in 2003, the Young Scientists' Prize from the Minister of Education, Culture, Sports, Science and Technology, Japan, in 2005, the Best Paper Award in 2007, the Best Letter Award from the IEICE Communications Society in 2009, and the IEICE Best Paper Award in 2016 and 2018. He is a Fellow of IEICE.

SHULABH GUPTA (Senior Member, IEEE) was born in Etah, India, in December 1982. He received the Bachelor of Technology (B.Tech.) degree in electronic engineering from the Indian Institute of Technology (Indian School of Mines), Dhanbad, India, in 2004, the Masters of Science (M.S.) degree in telecommunications from the Institut National de la Recherche Scientifique Energie Materiaux Telecommunications Research Center (INRS-EMT), Universite du Quebec, Montreal, QC, Canada, in 2006, and the Ph.D. degree in electrical engineering from the Ecole Polytechnique of Montreal, Montreal, QC, Canada, in 2012. His M.S. thesis research concerned optical signal processing related to the propagation of light in linear and nonlinear optical fibers and fiber Bragg gratings. His Ph.D. thesis research concerned analog signal-processing techniques using dispersion engineered structures.

From December 2009 to May 2010, he was a Visiting Research Fellow with the Tokyo Institute of Technology, Tokyo, Japan, where he was involved with the application of high impedance surfaces for oversized slotted waveguide antennas. He was a Postdoctoral Fellow with the University of Colorado Boulder, where he was working on the design and characterization of high-power UWB antennas. He joined The University of Hong Kong, from 2012 to 2014, as a Postdoctoral Fellow. He was a Postdoctoral Fellow with the Electrical Engineering Department, Ecole Polytechnique of Montreal, from April 2014 to January 2016. Since March 2016, he has been an Assistant Professor with the Department of Electronics (DoE), Carleton University, Ottawa. His research interests include multifunctional travelling-wave leaky-wave antennas for RFID and imaging applications. He was a recipient of the Young Scientist Award of EMTS Ottawa in 2007, URSI-GA, Chicago, in 2008, and ISAP, Jeju, in 2011. His thesis received the Best Doctoral Dissertation Award from the Ecole Polytechnique of Montreal in 2012, the Prix D'excellence de l'Association des Doyens des Etudes Superieures au Quebec (ADESAQ), Quebec, in 2013, and the Academic Gold Medal from the Governor General of Canada.